Studies of Vector Boson Scattering And Triboson Production with Delphes Parametrized Fast Simulation of Snowmass 2013

C. Degrande, O. Eboli, J. L. Holzbauer, S.-C. Hsu, A. Kotwal, S. Li, M. Marx, O. Mattelaer, J. Metcalfe, M-A. Pleier, C. Pollard, M. Rominsky, D. Wackeroth

September 11, 2013

1 Introduction

Multiboson production provides a unique way to probe Electroweak Symmetry Breaking (EWSB) and physics beyond the Standard Model (SM). With the discovery of the Higgs, it is easy to assume that EWSB happens according to the Higgs mechanism. In this case, the gauge couplings are completely specified and the gauge nature of the SM can be probed by studying vector boson scattering and anomalous gauge couplings. Any deviations from SM calculations gives clues to physics beyond the SM. Because the scale of this new physics is likely beyond the current experiment reach, we are motivated to use Effective Field Theory [1], using the Lagrangian shown in Equation 1.

$$\mathcal{L} = \mathcal{L}^{SM} + \sum_i \frac{c_i}{\Lambda^2}\mathcal{O}_i + \sum_j \frac{f_j}{\Lambda^4}\mathcal{O}_j \tag{1}$$

Where $\mathcal{O}_i$ are the dimension 6 operators, c_i represent the coupling constants, $\mathcal{O}_j$ are the dimension-8 operators and f_j represent the coupling constants. For this study, we tested both dimension 6 operators and dimension 8 operators. EFT satisfies unitarity and also has the benefit of being more predictive than the traditional method of looking at anomalous couplings.

This Snowmass exercise was performed using MadGraph [2] for event generation, Pythia for showering, a special version of Delphes [3] for the detector simulation and specially designed pile up files [4].

2 VBS $ZZ \to \ell\ell\ell\ell$

In this vector boson scattering channel, we explore anomalous production by studying the invariant mass distribution of the ZZ pair. The new physics is parameterized either by the following dimension-6 operator

$$\mathcal{L}_{\phi W} = \frac{c_{\phi W}}{\Lambda^2}\mathrm{Tr}(W^{\mu\nu}W_{\mu\nu})\phi^\dagger\phi \qquad (2)$$

or by one of the dimension-8 operators

$$\begin{aligned} \mathcal{L}_{T,8} &= \frac{f_{T8}}{\Lambda^4}B_{\mu\nu}B^{\mu\nu}B_{\alpha\beta}B^{\alpha\beta} \\ \mathcal{L}_{T,9} &= \frac{f_{T9}}{\Lambda^4}B_{\alpha\mu}B^{\mu\beta}B_{\beta\nu}B^{\nu\alpha} \end{aligned} \qquad (3)$$

where ϕ is the SM Higgs field, and $W^{\mu\nu}$ ($B^{\mu\nu}$) are the field strength tensors derived from the $SU(2)_L$ (Y) gauge fields. The fully-leptonic $ZZjj \to \ell\ell\ell\ell jj$ channel provides a fully reconstructible ZZ final state with small mis-identification backgrounds [5] which can be neglected in this sensitivity study. The contribution from jets accompanying non-VBS diboson production is reduced by requiring the forward jet-jet mass to be greated than 1 TeV. The dimension-8 operators mentioned above involve only the electrically-neutral gauge fields and therefore can be probed by the ZZ final state but not the WZ or WW final state.

MadGraph 1.5.10 is used for the generation of SM VBS and non-VBS processes as well as the non-SM processes mentioned above. Z bosons were required to decay to electron or muon pairs.

2.1 Event Selection

After Pythia 6.4 [6] parton showering, additional detector effects are applied using Delphes 3.0.9 [7] with the Snowmass parameterization [8, 4, 9, 10, 11]. Candidate VBS ZZ events are selected according to the following criteria:

- Exactly four selected leptons (each with $p_T > 25$ GeV) which can be separated into two opposite sign, same flavor pairs (No Z mass window requirement)
- At least two selected jets, each with $p_T > 50$ GeV
- $m_{jj} > 1$ TeV, where m_{jj} is the invariant mass of the two highest-p_T selected jets

2.2 Statistical Analysis

In order to determine the expected sensitivity to beyond-SM (BSM) ZZ contribution, the background-only p_0-value expected for signal+background is calculated using the $m_{4\ell}$ spectrum.

In order to show the improvement possible with the increased luminosity and center-of-mass energy, the 5σ discovery potential and 95% CL limits are studied. Since the $4-$lepton mass is the process $\sqrt{\hat{s}}$, the study of its distribution directly probes the energy-dependence of the new physics.

At sufficiently high energy, the amplitude predicted by higher-dimension operators will eventually violate unitarity. In this regime, the new physics that presumably restores unitarity is expected to be probed directly, such as the production of on-shell resonances. This is a very interesting regime because the masses and couplings of new resonances can be measured independently, which is a much more powerful probe as compared to the low-energy regime where only the appropriate ratio of coupling and mass can be probed. Furthermore, in the high energy regime it is also possible to study new decay modes of the resonances, whereas in the low-energy regime of EFT applicability we can only study the anomalous production of SM particles. The regime above the unitarity bound is probed more strongly by the higher energy colliders.

We present the sensitivity to the higher-dimension operators in two ways. In one case, we assume that the new physics is only probed "virtually" by higher-dimension operators involving SM fields, and in this case we require the generated events to lie below the unitarity bound in the diboson mass. In the second case, we allow the collider to probe the sensitivity to new physics above the unitarity bound through direct production of new resonances and measuring their masses, couplings and decay branching ratios. To display the latter physics potential, ideally we would use an ultraviolet-complete theory of strongly-interacting electroweak sector, which at the moment is not available. As a proxy for the additional physics that would be accessible in this high-energy regime, we also quote the sensitivity to the higher-dimension operators without making the unitarity bound requirement on the diboson mass.

The unitarity violation (UV) bounds are calculated using the form factor tool avaliable with VBFNLO [12]. The bounds, which are shown in Figure 1, vary as a function of the coefficients of the higher-dimension operators. Application of the bound lowers the sensitivity of the search, especially when the coefficient is large. We present the 5σ-significance discovery values and 95% CL limits with and without applying the UV bound in Table 1. Figures 4 shows the signal significance as a function of f_{T8}/Λ^4, f_{T9}/Λ^4 and $c_{\phi W}/\Lambda^2$ without the UV bound applied. The reconstructed 4-lepton invariant mass distribution are shown in Figure 2 and Figure 3 without and with the UV bound, respectively.

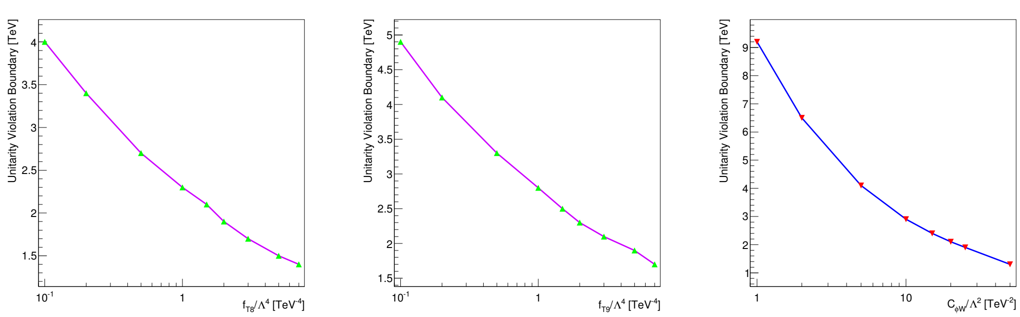

Figure 1: The unitarity violation boundaries of dimension-8 operators f_{T8}/Λ^4 (left), f_{T9}/Λ^4 (middle) and dimension-6 operator $C_{\phi W}/\Lambda^2$ (right) as functions of anomalous coupling coefficient values in $pp \to ZZ + 2j \to \ell\ell\ell\ell + 2j$ processes.

Parameter	dim.	Luminosity [fb^{-1}]	14 TeV		33 TeV	
			5σ	95% CL	5σ	95% CL
$c_{\phi W}/\Lambda^2$ [TeV^{-2}]	6	3000	16.2 (16.2)	9.7 (9.7)	13.2 (13.2)	8.2 (8.2)
		300	31.3 (31.5)	18.2 (18.3)	23.8 (23.8)	14.7 (14.7)
f_{T8}/Λ^4 [TeV^{-4}]	8	3000	2.9 (4.7)	1.7 (2.4)	1.6 (1.7)	1.0 (1.3)
		300	5.5 (8.4)	3.2 (5.3)	2.8 (2.3)	1.8 (1.8)
f_{T9}/Λ^4 [TeV^{-4}]	8	3000	5.7 (6.3)	3.9 (4.6)	3.8 (6.6)	2.5 (3.5)
		300	8.7 (9.0)	6.2 (6.7)	6.3 (10.1)	4.2 (8.2)

Table 1: In $pp \to ZZ + 2j \to \ell\ell\ell\ell + 2j$ processes, 5σ-significance discovery values and 95% CL limits for coefficients of high-dimension operators with 300 fb^{-1}/3000 fb^{-1} of integrated luminosity. To show the impact of the UV bound, the corresponding results are shown in parentheses.

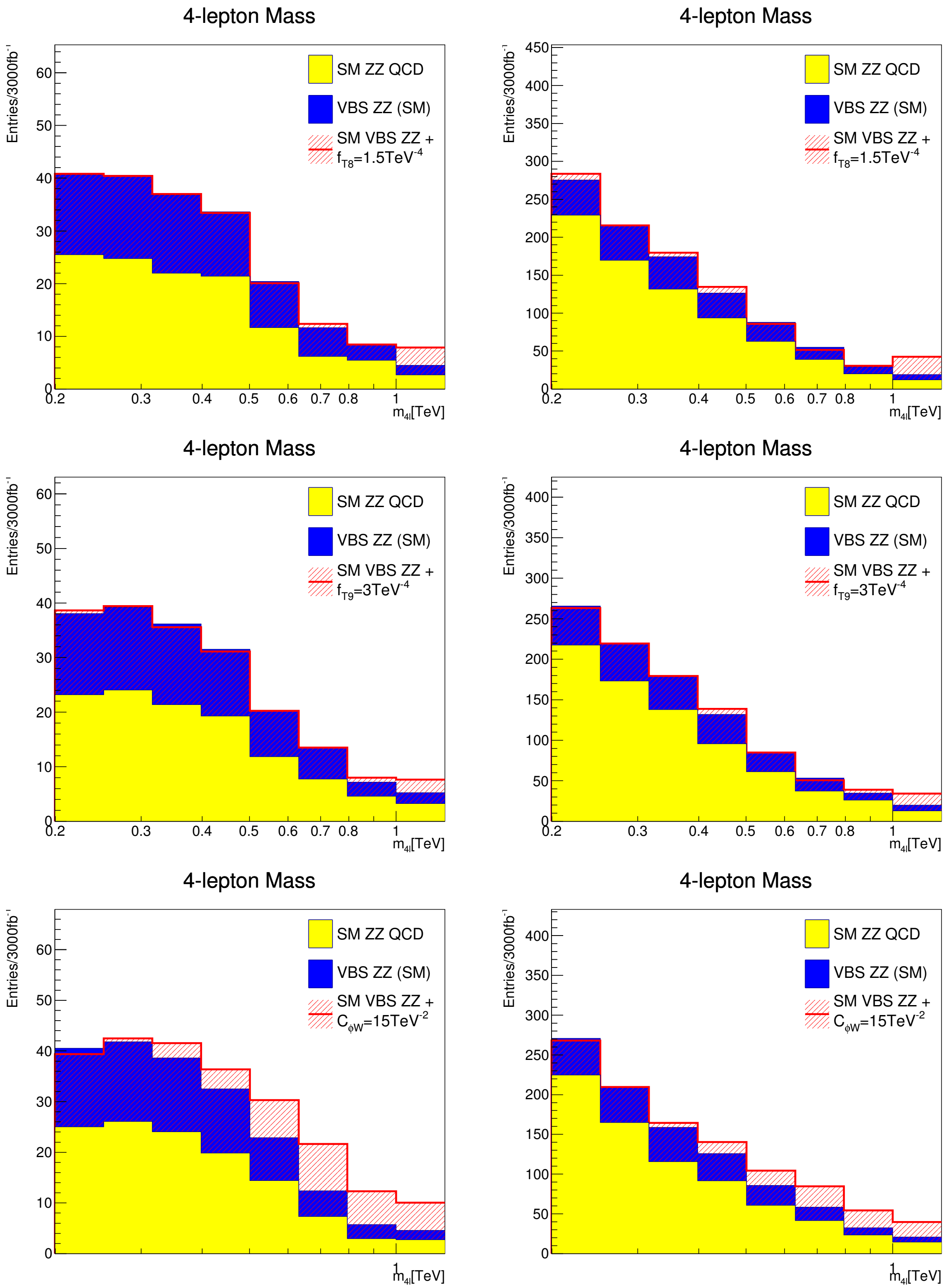

Figure 2: In the $pp \to ZZ + 2j \to \ell\ell\ell\ell + 2j$ process, the reconstructed 4-lepton mass ($m_{4\ell}$) spectrum comparisons between Standard Model and dimension-8 operator coefficient $f_{T8}/\Lambda^4 = 1.5TeV^{-4}$ (upper), $f_{T9}/\Lambda^4 = 3TeV^{-4}$ (middle) and dimension-6 operator coefficient $c_{\phi W}/\Lambda^2 = 15TeV^{-2}$ (bottom) are shown after requiring $m_{jj} >$ 1 TeV at $\sqrt{s} = 14$ TeV (left) and 33 TeV (right). The overflow and underflow bins are included in the plots. The UV bound is not applied.

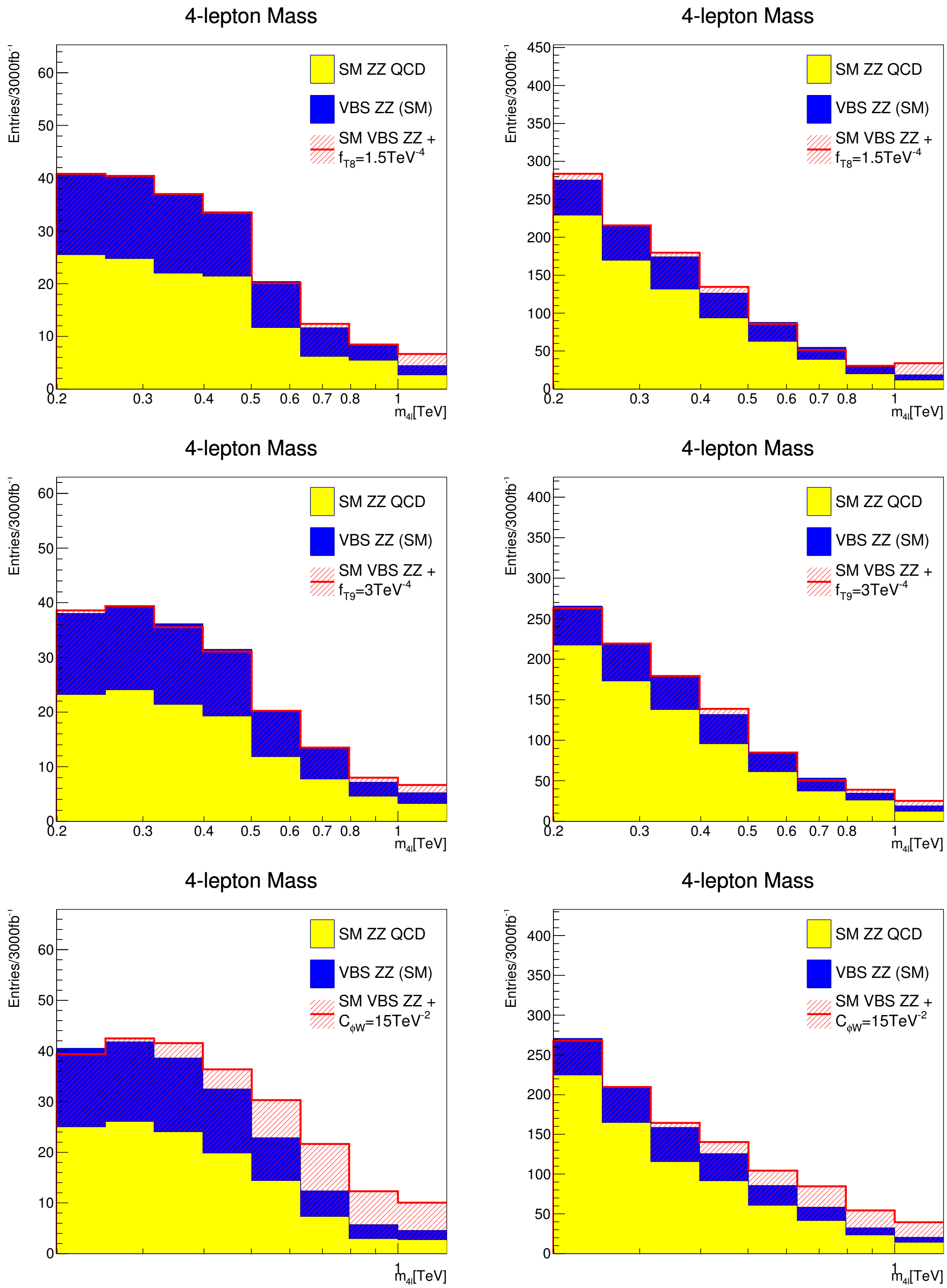

Figure 3: In the $pp \to ZZ + 2j \to \ell\ell\ell\ell + 2j$ process, the reconstructed 4-lepton mass ($m_{4\ell}$) spectrum comparisons between Standard Model and dimension-8 operator coefficient $f_{T8}/\Lambda^4 = 1.5TeV^{-4}$ (upper), $f_{T9}/\Lambda^4 = 3TeV^{-4}$ (middle) and dimension-6 operator coefficient $c_{\phi W}/\Lambda^2 = 15TeV^{-2}$ (bottom) are shown after requiring $m_{jj} >$ 1 TeV at $\sqrt{s} = 14$ TeV (left) and 33 TeV (right). The overflow and underflow bins are included in the plots. The UV bound is applied.

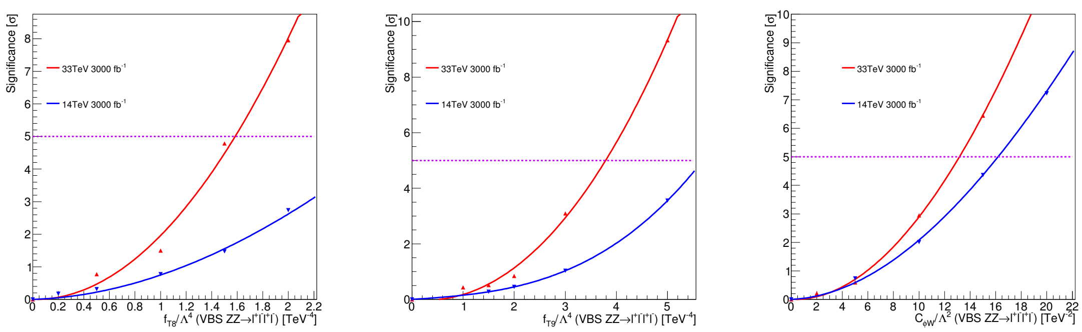

Figure 4: $pp \to ZZ + 2j \to \ell\ell\ell\ell + 2j$ signal significance as a function of f_{T8}/Λ^4 (left), f_{T9}/Λ^4 (middle) and $c_{\phi W}/\Lambda^2$ (right) calculated from reconstructed ZZ mass spectra at $\sqrt{s} = 14$ TeV and 33 TeV. The UV bound is not applied.

3 VBS $WZ \to \ell\nu\ell\ell$

We parameterize new physics in this channel using the dimension-8 operator

$$\mathcal{L}_{T,1} = \frac{f_{T1}}{\Lambda^4} \mathrm{Tr}[\hat{W}_{\alpha\nu}\hat{W}^{\mu\beta}] \times \mathrm{Tr}[\hat{W}_{\mu\beta}\hat{W}^{\alpha\nu}] \quad (4)$$

and dimension-6 operator

$$\mathcal{L}_{\phi d} = \frac{c_{\phi d}}{\Lambda^2} \partial_\mu(\phi^\dagger\phi)\partial^\mu(\phi^\dagger\phi) \quad (5)$$

The fully leptonic $WZjj \to \ell\nu\ell\ell jj$ channel can be reconstructed by solving for the neutrino p_z using the W boson mass constraint. Its cross section is larger than that of $ZZjj \to \ell\ell\ell\ell jj$ and it can probe some operators better than the latter process. The electron and muon decay channels are used in this study. Mis-identification backgrounds are small in this channel, as shown in [13] and therefore neglected in this sensitivity study. The lepton from W decay must be identified in order to use the W mass constraint. The procedure described in [14, 15] is also used here.

Non-VBS WZ production in association with initial-state radiation of two jets was simulated using MadGraph [2]. MadGraph 1.5.10 was used to generate SM and non-SM VBS WZ production.

3.1 Event Selection

After Pythia 6.4 [6] parton showering, additional detector effects are applied using Delphes 3.0.9 [7] with the Snowmass parameterization [8, 4, 9, 10, 11]. Events are considered VBS WZ candidates provided they meet the following criteria:

- Exactly three selected leptons (each with $p_T > 25$ GeV) which can be separated into an opposite sign, same flavor pair and an additional single lepton
- At least two selected jets with $p_T > 50$ GeV
- $m_{jj} > 1$ TeV, where m_{jj} is the invariant mass of the two highest-p_T selected jets

3.2 Statistical Analysis

The statistical analysis is identical to that employed in Sec. 2.2. As with the VBS ZZ channel, we present sensitivity studies with and without the UV bound applied. The bounds for different operators are shown in Figure 5. To show the impact of the UV bound, we present the 5σ-significance discovery values and 95% CL limits both without and with (in parentheses) the UV bounds applied, in Table 2. Figure 8 shows the signal significance as a function of f_{T1}/Λ^4 and $c_{\phi d}/\Lambda^2$ without the UV bound and the corresponding reconstructed 4-lepton invariant mass distributions are shown in Figure 6. The same distributions with the UV bounds are shown in Figure 7.

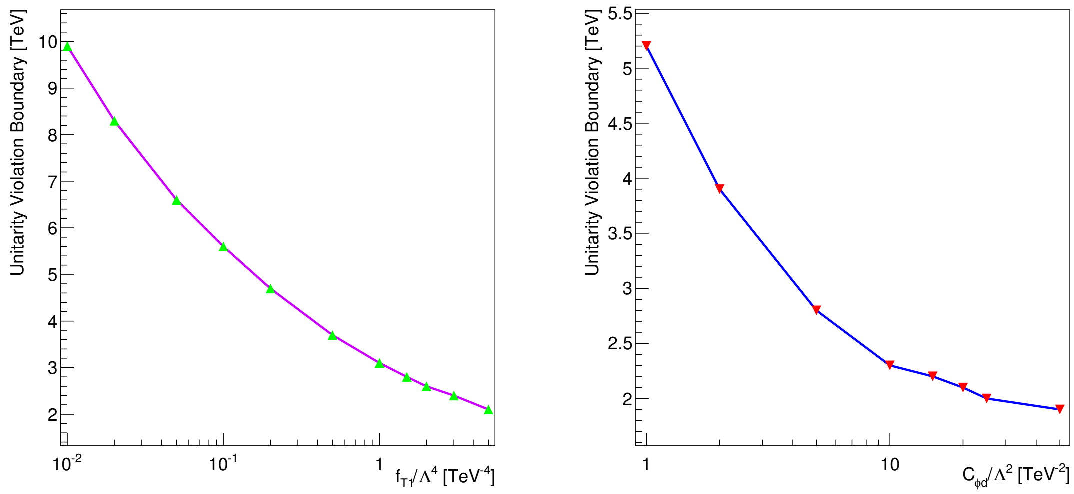

Figure 5: The unitarity violation boundaries of dimension-8 operator f_{T1}/Λ^4 (left) and dimension-6 operator $C_{\phi d}/\Lambda^2$ (right) as functions of anomalous coupling coefficient values in $pp \to WZ + 2j \to \ell\nu\ell\ell + 2j$ processes.

Parameter	dim.	Luminosity [fb^{-1}]	14 TeV		33 TeV	
			5σ	95% CL	5σ	95% CL
$c_{\phi d}/\Lambda^2$ [TeV^{-2}]	6	3000	15.2 (15.2)	9.1 (9.1)	12.6 (12.7)	7.7 (7.7)
		300	28.5 (28.7)	17.1 (17.1)	23.1 (23.3)	14.1 (14.2)
f_{T1}/Λ^4 [TeV^{-4}]	8	3000	0.6 (0.9)	0.4 (0.5)	0.3 (0.6)	0.2 (0.3)
		300	1.1 (1.6)	0.7 (1.0)	0.6 (0.9)	0.3 (0.6)

Table 2: In $pp \to WZ+2j \to \ell\nu\ell\ell+2j$ processes, 5σ-significance discovery values and 95% CL limits for coefficients of higher-dimension operators with 300 fb^{-1}/3000 fb^{-1} of integrated luminosity at 14 TeV and 33 TeV. The results obtained after applying the UV bounds are shown in parentheses.

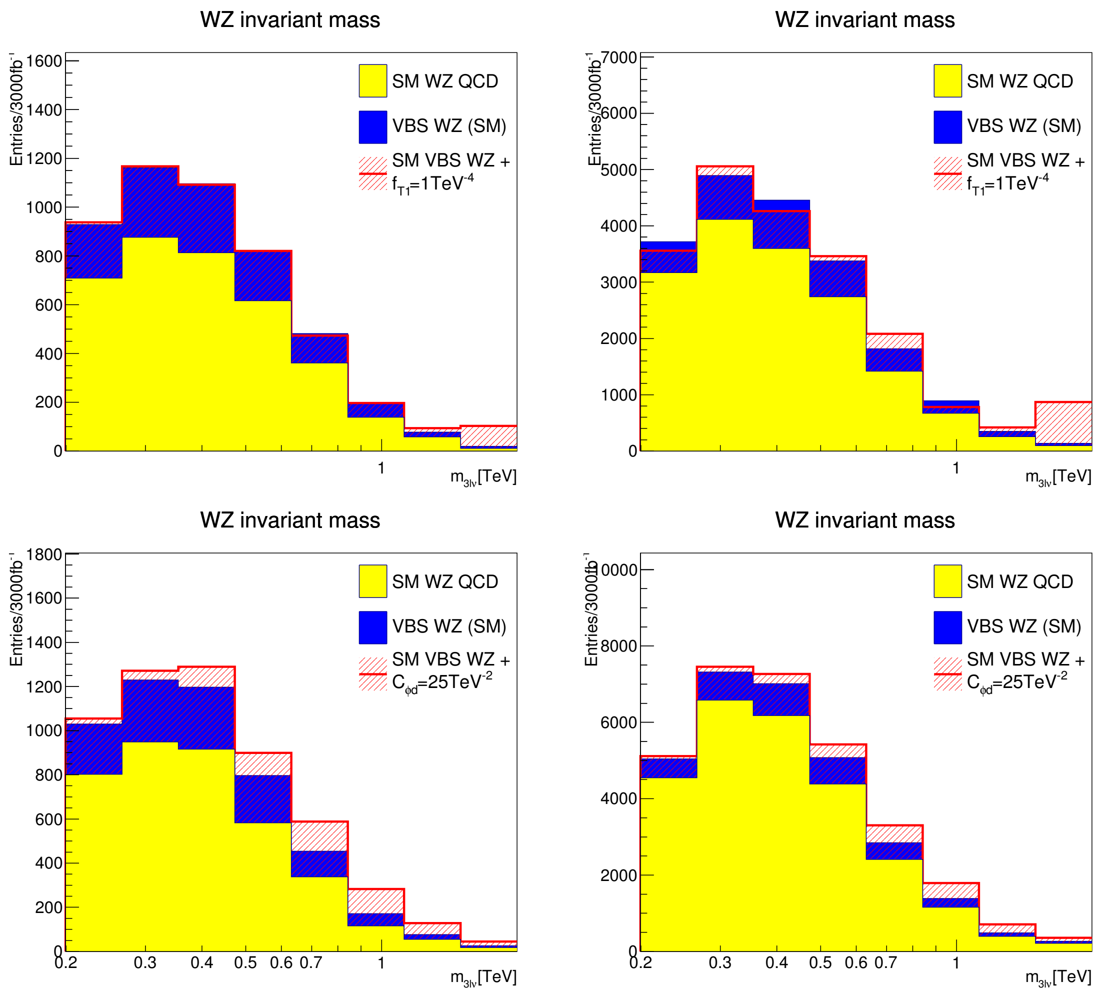

Figure 6: In the $pp \to WZ + 2j \to \ell\nu\ell\ell + 2j$ channel, the reconstructed WZ mass spectrum comparisons between Standard Model and dimension-8 operator coefficient $f_{T1}/\Lambda^4 = 1$ TeV^{-4} (upper) and dimension-6 operator coefficient $c_{\phi d}/\Lambda^2 = 25\text{TeV}^{-2}$ (bottom) are shown using the charged leptons and the neutrino solution after requiring $m_{jj} > 1$ TeV at $\sqrt{s} = 14$ TeV (left) and 33 TeV (right). The overflow and underflow bins are included in the plots. The UV bounds have not been applied.

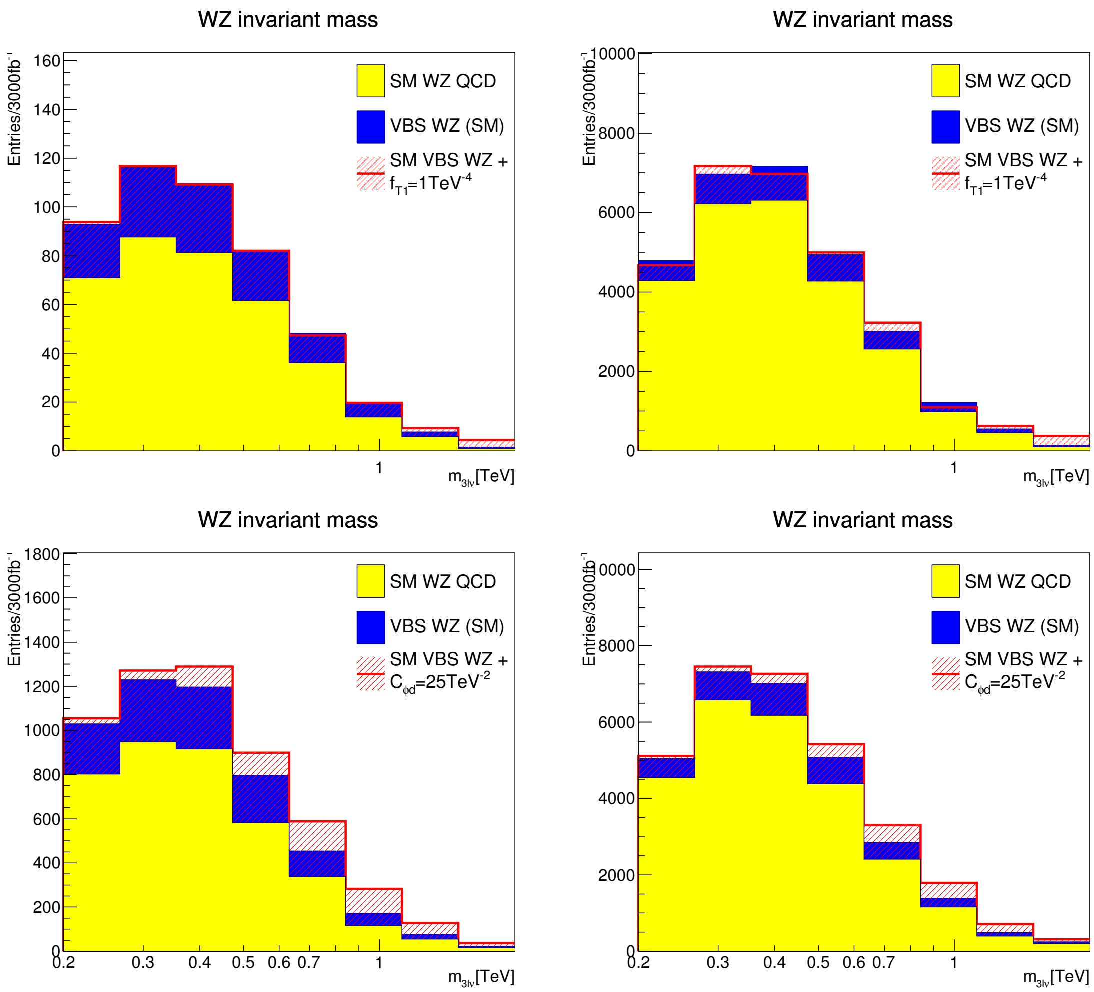

Figure 7: In the $pp \to WZ + 2j \to \ell\nu\ell\ell + 2j$ channel, the reconstructed WZ mass spectrum comparisons between dimension-8 operator coefficient $f_{T1}/\Lambda^4 = 1TeV^{-4}$ (upper), dimension-6 operator coefficient $c_{\phi d}/\Lambda^2 = 25TeV^{-2}$ (bottom) and Standard Model are shown using the charged leptons and the neutrino solution after requiring $m_{jj} > 1$ TeV at $\sqrt{s} = 14$ TeV (left) and 33 TeV (right). The overflow and underflow bins are included in the plots. The UV bounds have been applied.

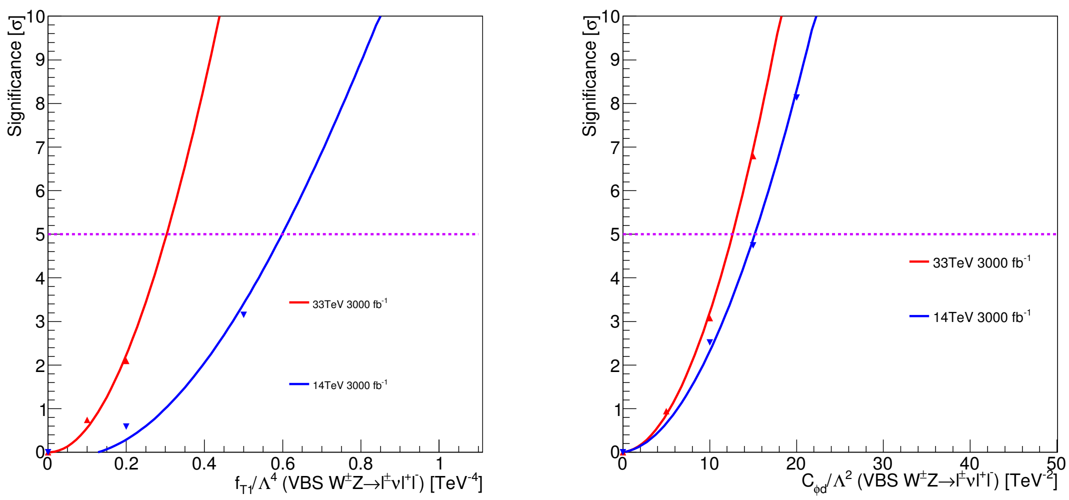

Figure 8: $pp \to WZ + 2j \to \ell\nu\ell\ell + 2j$ signal significance as a function of f_{T1}/Λ^4 (left) and $c_{\phi d}/\Lambda^2$ (right) calculated from reconstructed WZ mass spectra at $\sqrt{s} = 14$ TeV and 33 TeV. The UV bounds have not been applied.

4 VBS $W^\pm W^\pm \to \ell\nu\ell\nu$

The sensitivity to new physics was examined in the $pp \to W^\pm W^\pm + 2j \to \ell\nu\ell\nu + 2j$ (ssWW) channel where l is an electron or muon. The dimension-8 operator, f_{T1}/Λ^4 as shown in 6, was used to probe deviations from SM predictions.

$$\mathcal{L}_{T,1} = \frac{f_{T1}}{\Lambda^4}\mathrm{Tr}[\hat{W}_{\alpha\nu}\hat{W}^{\mu\beta}] \times \mathrm{Tr}[\hat{W}_{\mu\beta}\hat{W}^{\alpha\nu}] \tag{6}$$

A range of values surrounding a 5σ significance level were studied for 14 TeV and 100 TeV pp machine scenarios for various pileup conditions. The effect of a Unitarity Violation (UV) cutoff was also considered.

4.1 Monte Carlo Predictions

The samples were generated using MadGraph version 5.1.5.11. Samples were produced for backgrounds, SM VBS, and new physics. The main backgrounds in ssWW VBS production (sensitive to aQGC) are ssWW QCD diagrams, WZ, $W\gamma$, and mis-identification backgrounds including charge mis-identification. The $W\gamma$ and mis-identification backgrounds were assumed to have the same shape as the WZ background, therefore, the WZ background was scaled appropriately (factor of 2) to account for these other backgrounds as well. The samples were showered via the Snowmass Delphes showering tool [9, 10, 11] that implemented various machine energies and pileup scenarios.

4.2 Event Selection

After Pythia 6.4 [6] parton showering, additional detector effects are applied using Delphes 3.0.9 [7] with the Snowmass parameterization [8, 4, 9, 10, 11]. The analysis selection of the VBS ssWW candidates were given by the following criteria:

- Single lepton trigger fired
- Exactly two leptons of same sign each with $p_T > 25$ GeV
- At least two jets with $p_T > 50$ GeV.
- $m_{jj} > 1$ TeV, where m_{jj} is the invariant mass of the two highest-p_T jets

The high jet p_T cut helps protect against pileup jets while the m_{jj} cut strongly selects for the VBS signal region.

The amplitude for ssWW VBS violates unitarity at high mass when the higher dimension operators are included. One method of imposing unitarity preservation is to apply a unitarity-violation (UV) bound as an upper bound on the invariant mass of the WW pair at truth-level. The bound was calculated using a tool developed by the VBFNLO authors. This tool was used to calculate the UV bound for each f_{T1}/Λ^4 and beam energy used in this study. Figure 9 shows the UV bounds for both 14 TeV and 100 TeV used in this analysis. As expected, when f_{T1}/Λ^4 approaches zero the bound goes to infinity, since the SM amplitude respect unitarity at all energies.

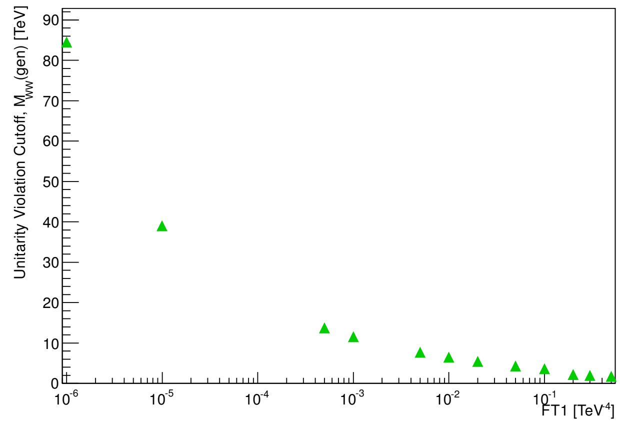

Figure 9: The Unitarity Violation (UV) cut-off values for a given f_{T1}/Λ^4.

4.3 Statistical Analysis

The 4-body invariant mass of the two leading jets and the two leptons, m_{jjll}, was used to discriminate new physics from the SM. The statistical analysis approach is identical to that in Sec. 2.2.

Figure 10 compares the shape of the m_{jjll} distributions for the SM and two values of f_{T1}/Λ^4 (0.1 TeV^{-4} and 0.2 TeV^{-4} respectively) at 14 TeV. Increasing the anomalous quartic coupling increases the event rate at the high end of the m_{jjll} spectrum. A similar plot for 100 TeV is shown in Figure 11 for $f_{T1}/\Lambda^4 = 0.001$ TeV^{-4}.

The different pileup scenarios as well as the effect of the UV bound is shown in Figure 12 for different pp collider energies. The pileup has a small, but non-negligible effect whereas the UV bound has a larger effect. Applying the UV bound is a conservative method and is presented in Table 3 in parentheses.

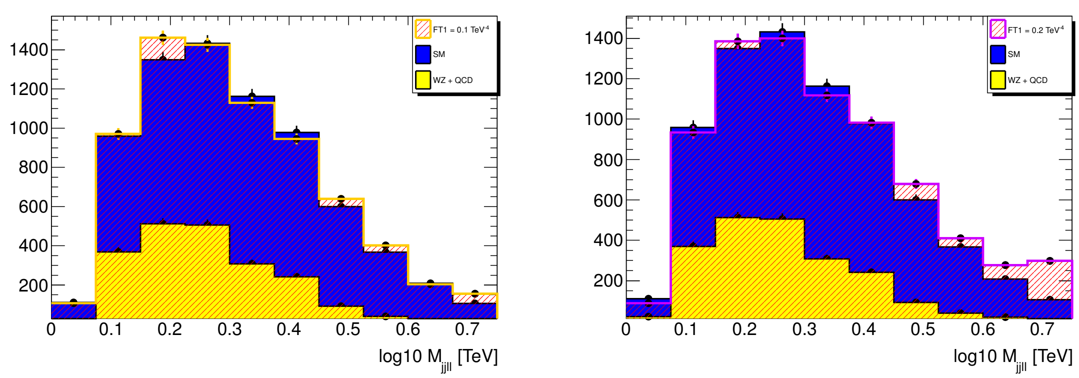

Figure 10: The invariant mass of the 4-body m_{jjll} system in ssWW events is shown for f_{T1}/Λ^4 equal to 0.1 TeV^{-4} corresponding to a significance of 4.2σ (Frequentist method) (left) and $f_{T1}/\Lambda^4 = 0.2$ with 17σ significance (LLR method) (right) for 14 TeV beam energy, 140 pileup events per crossing, without the UV cut-off applied, and 3000 fb^{-1} scenario.

A summary of the 5σ significance and the 95% Confidence Level (CL) for each machine scenario is listed in Table 3 along with a direct comparison of 14 TeV and

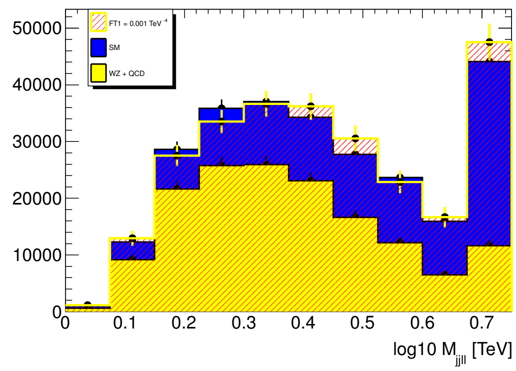

Figure 11: In ssWW events, m_{jjll} for $f_{T1}/\Lambda^4 = 0.001$ corresponding to a 4σ significance for the case of a 100 TeV pp machine with 263 pileup, without the UV cut-off applied, at 3000 fb^{-1} is shown.

100 TeV machines at 3000 fb^{-1} for zero pileup. At 14 TeV by running 3000 fb^{-1} compared to 300 fb^{-1} the 5σ limit on f_{T1}/Λ^4 is 2 times lower. However, with the UV cut-off the limit can be set almost 2 times lower. The direct comparison of data without pileup indicates at least a factor of 100 gain in sensitivity to the operator f_{T1}/Λ^4 for a 5σ discovery potential jumping from a 14 TeV machine to a 100 TeV machine.

Parameter	$\sqrt{s}$ [TeV]	Luminosity [fb^{-1}]	pileup [events/crossing]	5σ [TeV^{-4}]	95% CL [TeV^{-4}]
f_{T1}/Λ^4	14	300	50	0.2 (0.4)	0.1 (0.2)
f_{T1}/Λ^4	14	3000	140	0.1 (0.2)	0.06 (0.1)
f_{T1}/Λ^4	14	3000	0	0.1 (0.2)	0.06 (0.1)
f_{T1}/Λ^4	100	1000	40	0.001 (0.0009)	0.0004 (0.0004)
f_{T1}/Λ^4	100	3000	263	0.001 (0.001)	0.0008 (0.0007)
f_{T1}/Λ^4	100	3000	0	0.001 (0.001)	0.0008 (0.0007)

Table 3: In $pp \to W^\pm W^\pm + 2j \to \ell\nu\ell\nu + 2j$ processes, 5σ-significance discovery values and 95% CL limits are shown for coefficients the higher-dimension operator, f_{T1}/Λ^4, for different machine scenarios without the UV cut and with the UV cut in parenthesis.

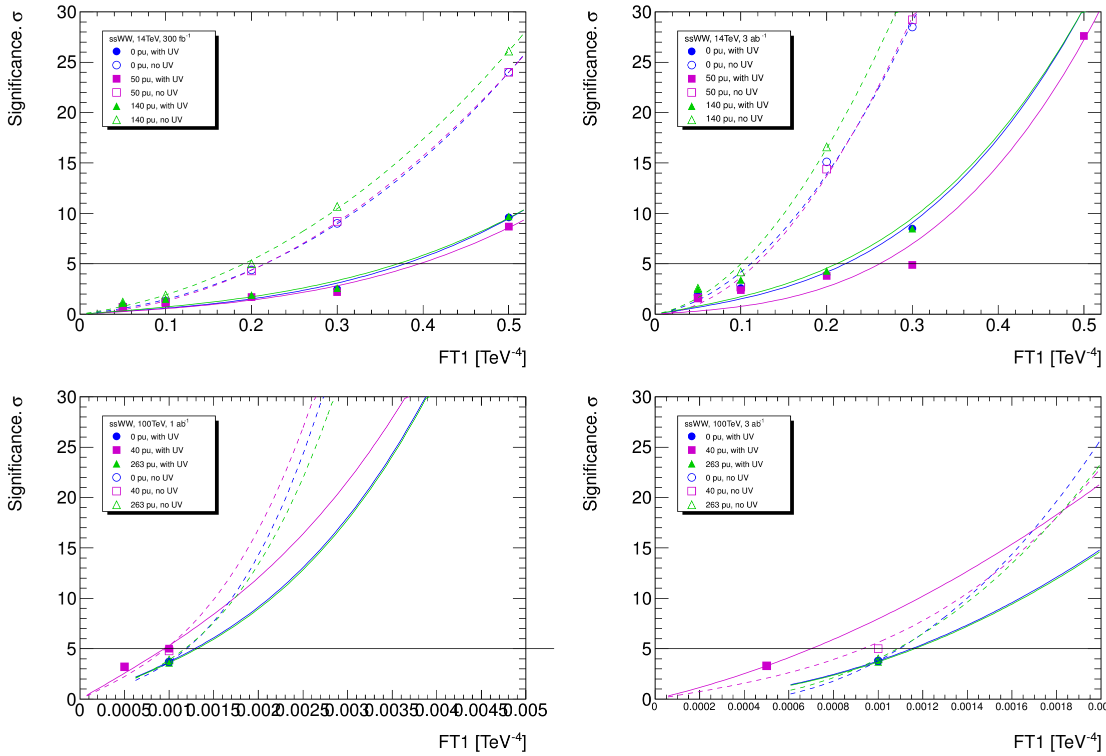

Figure 12: The significance trends for each beam energy and luminosity are shown for the various pileup scenarios. The fits are done with a 3rd order polynomial (lines). For the each set of machine conditions, each pileup scenario was considered with (solid points/lines) and without (open points/dashed lines) the Unitarity Violation cut-off. The top row displays the 14 TeV cases at 300 fb^{-1} (left) and 3000 fb^{-1} (right). The bottom row shows 100 TeV cases at 1000 fb^{-1} (left) and 3000 fb^{-1} (right).

5 $WWW \to \ell\nu\ell\nu\ell\nu$

In the Standard Model (SM), the only allowed quartic coupling terms in the Lagrangian are $WWWW$, $WWZZ$, $WWZ\gamma$ and $WW\gamma\gamma$, and they are completely specified. Measuring these couplings will provide stringent tests on the SM and guide searches on physics beyond the SM. These couplings can be measured using triboson production as well as vector boson scattering. The triboson WWW production probes the $WWWW$ coupling, while WWZ and $WW\gamma$ production probe the $WWZZ, WWZ\gamma$ and $WW\gamma\gamma$ couplings respectively [16]. This section describes a cross section scan of WWW, WWZ, WZZ and ZZZ production for different anomalous couplings induced by higher-dimension operators, followed by a case study of WWW for both dimension-8 and dimension-6 operators.

The dimension-8 operator studied most extensively was the $\mathcal{L}_{T,0}$ operator, given below

$$\mathcal{L}_{T,0} = \frac{f_{T,0}}{\Lambda^4}\mathrm{Tr}[\hat{W}_{\mu\nu}\hat{W}^{\mu\nu}] \times \mathrm{Tr}[\hat{W}_{\alpha\beta}\hat{W}^{\alpha\beta}] \quad (7)$$

The dimension-6 operator used is $\mathcal{L}_{WWW}$, given below

$$\mathcal{L}_{WWW} = \frac{C_{WWW}}{\Lambda^2}\mathrm{Tr}[W_{\mu\nu}W^{\nu\rho}W^{\mu}_{\rho}] \quad (8)$$

5.1 Monte Carlo Predictions

MadGraph 1.5.11 [2] was used to generate all WWW, WWZ, WZZ and ZZZ samples and background samples. In all cases W and Z bosons were required to decay leptonically to electrons or muons. Default generator cuts were applied:

- jet $p_T > 20$ GeV
- lepton $p_T > 10$ GeV
- photon $p_T > 10$ GeV
- jet $|\eta| < 5$
- lepton & photon $|\eta| < 2.5$

We performed a cross section scan to compare the SM cross sections to anomalous coupling cross sections for various higher dimension operators (Table 5.1 and Table 5.1). From the study, the $\mathcal{L}_{T0}$ operator is found to have the largest effect on triboson production from the dimension-8 operators, and $\mathcal{L}_{WWW}$ from the dimension-6 operators, particularly in the WWW channel. For this reason, we focus on this channel and these operators for the remainder of this section.

5.2 Event Selection

After Pythia 6.4 [6] parton showering, additional detector effects are applied using Delphes 3.0.9 [7] with the Snowmass parameterization [8, 4]. This parameterization includes effects from pile-up events. We have studied these effects and found them to be negligible for this analysis, which focuses on events with high invariant mass.

operator	WWW	WWZ	WZZ	ZZZ
SM cross section (ab)	603.4	124.2	9.634	0.972
$\mathcal{L}_{S0}$/SM	1.0	1.0	1.0	1.0
$\mathcal{L}_{S1}$/SM	1.0	1.0	1.0	1.0
$\mathcal{L}_{M0}$/SM	1.46	1.09	1.05	1.02
$\mathcal{L}_{M1}$/SM	1.17	1.02	1.04	1.03
$\mathcal{L}_{M2}$/SM	1.0	1.05	1.0	1.02
$\mathcal{L}_{M3}$/SM	1.0	1.01	1.00	1.01
$\mathcal{L}_{T0}$/SM	18.31	3.96	3.38	2.90
$\mathcal{L}_{T1}$/SM	15.15	2.10	2.83	2.90
$\mathcal{L}_{T2}$/SM	4.48	1.32	1.35	1.54
$\mathcal{L}_{T8}$/SM	1.0	1.0	1.0	1.31
$\mathcal{L}_{T9}$/SM	1.0	1.0	1.0	1.08

Table 4: The ratios of cross sections for various dimension-8 operators to SM values for a 14 TeV pp collider. In each case, the coefficient of the dimension-8 operator was set to 10 TeV^{-4}. All channels are fully leptonic decays.

operator	WWW	WWZ	WZZ	ZZZ
SM cross section (ab)	603.4	124.2	9.634	0.972
$\mathcal{L}_{WWW}$/SM	1.4	1.3	1.4	1.0
$\mathcal{L}_{W}$/SM	1.1	1.1	1.2	1.1
$\mathcal{L}_{b}$/SM	1.0	1.0	1.0	1.0

Table 5: The ratios of cross sections for various dimension-6 operators to SM values for a 14 TeV pp collider. In each case, the coefficient of the dimension-6 operator was set to 5 TeV^{-2}. All channels are fully leptonic decays.

Thus, all results presented in this section are extracted using Monte Carlo events generated with the no pile-up, in the interest of reducing computational time.

Events are considered to be part of the WWW signal if they meet the following criteria, where $p_T(\ell)$ is the transverse momentum of the lepton, $M(\text{all lep})$ is the invariant mass of all the leptons with $p_T(\ell) > 25$ GeV and $E_{\mathrm{T}}^{\mathrm{miss}}$ is the missing transverse energy of the event:

- At least three leptons where leptons must have $p_T(\ell) > 25$ GeV
- No two leptons may have the same flavor and opposite charge (to suppress diboson WZ background)
- $M(\text{all lep}) > 400$ GeV
- $E_{\mathrm{T}}^{\mathrm{miss}} > 150$ GeV

These selections were specifically chosen to optimize the signal and reduce backgrounds. The backgrounds considered include Z+jets, W+2jets, $t\bar{t}$, diboson (WW, WZ, ZZ), and $Z+\gamma$. The first two selections are extremely useful in reducing backgrounds to allow the signal to be studied. The first reduces particularly W+jets, Z+jets and WW, and the second reduces backgrounds with Z bosons. The selection on lepton number also helps to reduce the $t\bar{t}$ background, but as only one jet has to fake a lepton and the cross-section for this process is much higher than the signal process, we still have a comparatively large contribution from $t\bar{t}$. The last two selections help to reduce this remaining $t\bar{t}$ contamination. After these selections, the results are not significantly affected by the remaining events and these background processes are neglected in the final analysis.

There is an additional selection at the parton (truth) level to remove events in the kinematic region where the amplitude would violate unitarity. Events are removed if the invariant mass of the three true W bosons is larger than the unitarity bound. These bounds are estimated using the form factor tool avaliable with VBFNLO [12] and are presented for various values of f_{T0}/Λ^4 and C_{WWW}/Λ^2 in Figure 13. The bound rises rapidly for lower values of these coefficients, leading to a reduced impact of this bound. Conversely, for higher values of the coefficients, where the cross-section is higher, the impact of this bound is stronger.

In the next section, for both $\mathcal{L}_{T0}$ and $\mathcal{L}_{WWW}$ operators, we present results without the unitarity bound applied. We also comment on expectations with the removal of unitarity events under the scheme we have just discussed in Section 5.3.1.

5.3 Statistical Analysis

The distribution of $M(\text{all lep})$ is used for hypothesis testing. We compare the standard model prediction with the prediction for a non-zero value of a given higher-dimension operator. The statistical analysis is identical to that employed in Sec. 2.2. Figure 16 shows the WWW templates used for the 33 TeV pp collider, before the lepton invariant mass selection. The significance estimate uses distributions with this cut applied and different binning depending on the machine energy. Figure 15 shows the significance estimates for various f_{T0} and C_{WWW} values for different hadron collider

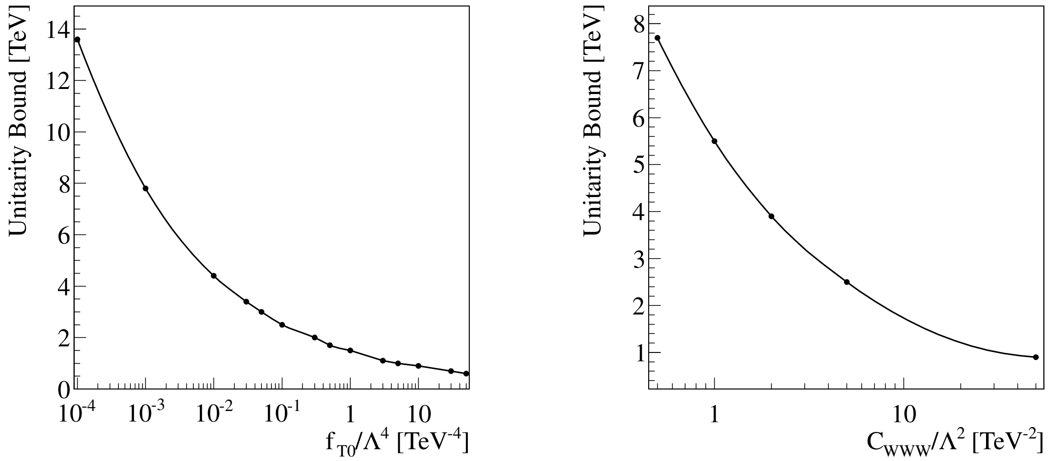

Figure 13: Unitarity bounds for the f_{T0} operator (left) and for the C_{WWW} operator (right) in various scenarios.

machines being studied for Snowmass. As the machine energies and integrated luminosities increase we are able to put tighter constraints on these operators, and of course we are also able to discover and probe new physics at increasingly higher mass scales and/or smaller couplings.

In this section we do not apply the UV bound. This bound may be applied as a cut on the generator-level WWW mass and there may be other ways to impose unitarity preservation that are less severe. To give a sense of the range of possibilities, we discuss in Sec. 5.3.1 what might happen if a simple UV bound is applied.

Table 6 gives the approximate 5σ-significance discovery values for the $\mathcal{L}_{T0}$ operator coefficient for different pp colliders.

	$300\,\mathrm{fb}^{-1}$	$1000\,\mathrm{fb}^{-1}$	$3000\,\mathrm{fb}^{-1}$
$\sqrt{s} = 14$	1.2 TeV^{-4}	-	0.6 TeV^{-4}
$\sqrt{s} = 33$	-	-	0.05 TeV^{-4}
$\sqrt{s} = 100$	-	0.004 TeV^{-4}	0.002 TeV^{-4}

Table 6: Summary of expected sensitivity to anomalous WWW production at various hadron collider machines, without the application of the UV bound, quoted in the terms of 5σ-significance discovery values of f_{T0}/Λ^4.

Table 7 gives the approximate 5σ-significance discovery values for the C_{WWW} operator for different pp colliders.

5.3.1 Comment on the Impact of the Unitarity Violation Selection

As mentioned previously, we want to consider what happens when unitarity violating events are removed, which can be done in different ways. Here, we apply a selection on the generator-level WWW mass using the values discussed in Section 5.2. Figure 16 shows the WWW templates used for the 33 TeV machine, before the lepton invariant

	300 fb^{-1}	1000 fb^{-1}	3000 fb^{-1}
$\sqrt{s} = 14$	4.8 TeV^{-2}	-	2.3 TeV^{-2}
$\sqrt{s} = 33$	-	-	1.7 TeV^{-2}
$\sqrt{s} = 100$	-	1.3 TeV^{-2}	0.9 TeV^{-2}

Table 7: Summary of expected sensitivity to anomalous WWW production at various hadron collider machines, without the application of the UV bound, quoted in the terms of 5σ-significance discovery values of C_{WWW}/Λ^2.

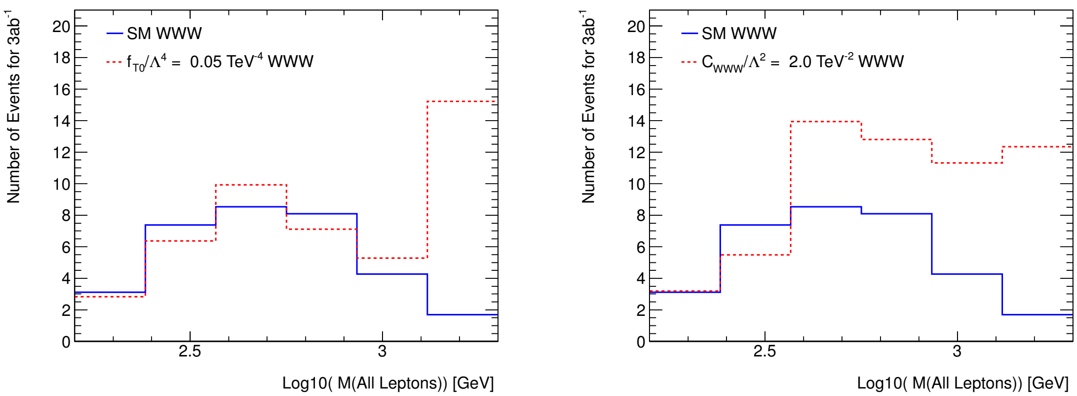

Figure 14: WWW invariant mass of all leptons without applying the UV bound, for the SM and with $f_{T0}/\Lambda^4 = 0.05$ TeV^{-4} (left) and $C_{WWW}/\Lambda^2 = 2\ TeV^{-2}$ (right) for $\sqrt{s} = 33$ TeV. This distribution was made without the lepton invariant mass selection.

mass selection for the same operator and coefficient, with and without the unitarity violation selection applied for f_{T0}. The lower number of events in the last bin of the first figure is due to the unitarity violating event removal. The unitarity violation criteria used in this study has a large impact on the f_{T0} results with this simple event removal, increasing the values from Table 6 of f_{T0}/Λ^4 at which we might expect a 5σ-significance discovery by more than a factor of 20.

The impact of the removal of unitarity violation events under the scheme used in this document is less severe for the C_{WWW} operator. Figure 17 shows the WWW templates used for the 33 TeV machine, before the lepton invariant mass selection for the same operator and coefficient, with and without the unitarity violation selection applied for C_{WWW}. There are fewer events in the last bins of Figure 17 due to the application of the extra selection, but overall the distributions are relatively similar, much more so than for f_{T0} (see Figure 16). Figure 18 shows the significance estimates for various C_{WWW} values for 5 different hadron collider machines being studied for Snowmass, with unitarity violating events removed. These values are generally 10 to 20% higher than then values of f_{T0}/Λ^4 at which we might expect a 5σ-significance discovery without the removal of these events.

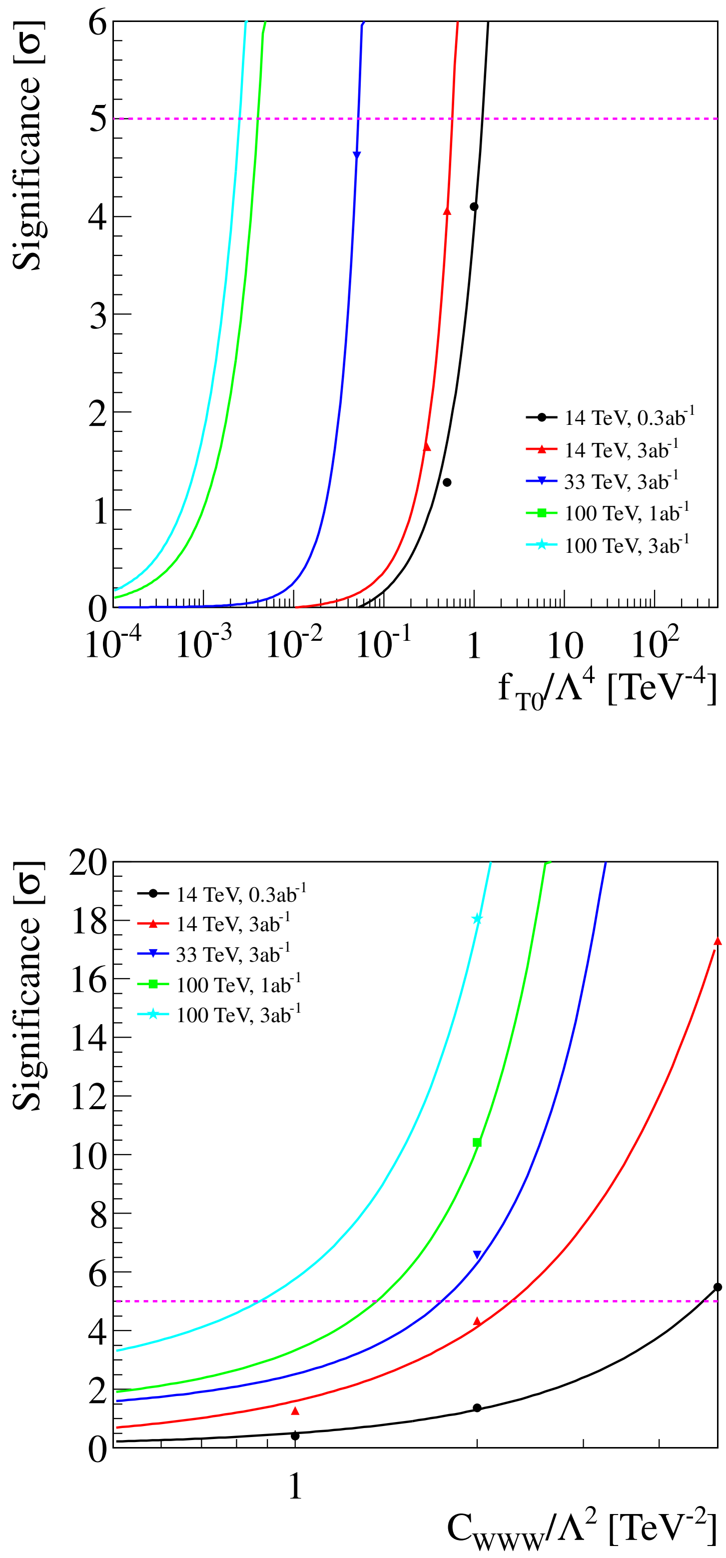

Figure 15: Significance values without the application of the UV bound as a function of f_{T0}/Λ^4 (top) and C_{WWW}/Λ^2 (bottom) in various scenarios.

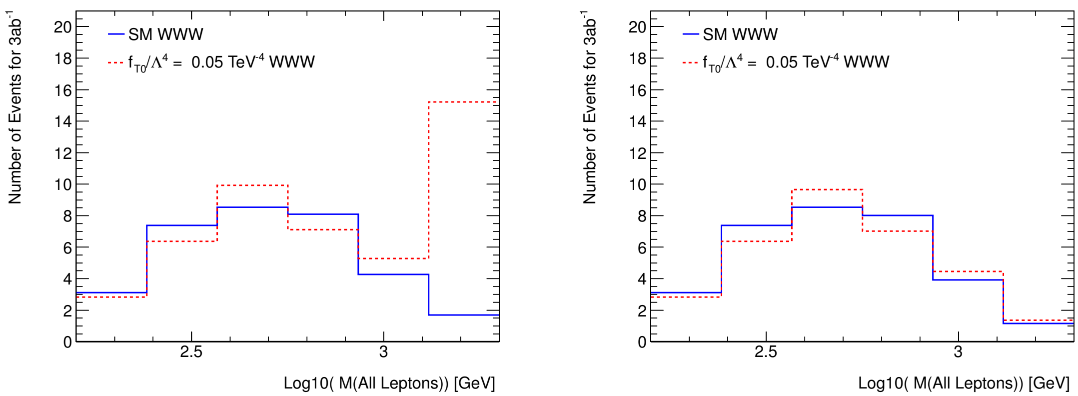

Figure 16: WWW invariant mass of all of the leptons for the WWW SM and WWW with f_{T0} of 0.05 TeV^{-4} for $\sqrt{s} = 33$ TeV without the unitarity violation selection (left) and with this selection applied (right). This distribution was made without the lepton invariant mass selection.

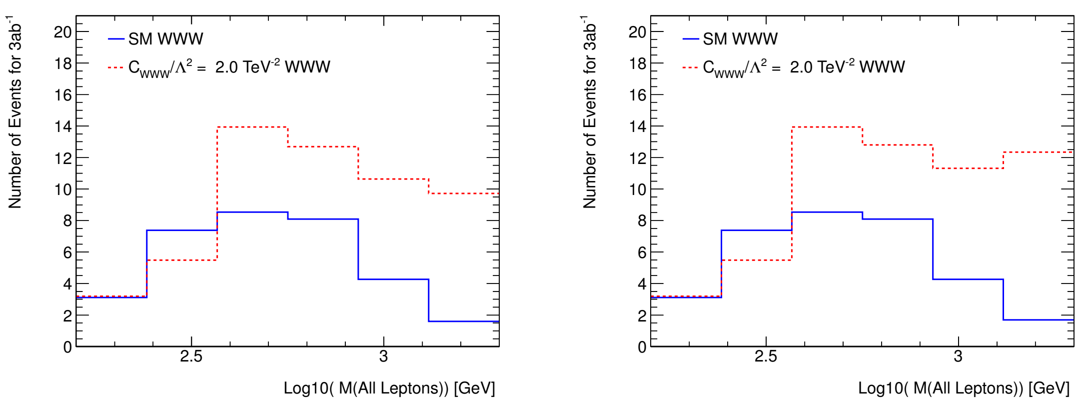

Figure 17: Invariant mass of all of the leptons for the WWW SM and WWW with C_{WWW} of 2 TeV^{-2} for $\sqrt{s} = 33$ TeV without the unitarity violation selection (left) and with this selection applied (right). This distribution was made without the lepton invariant mass selection.

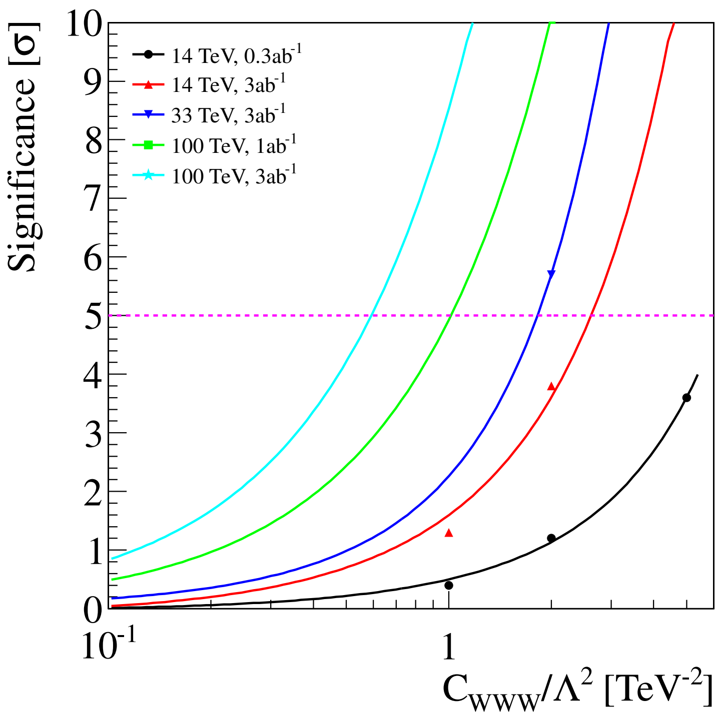

Figure 18: Significance values for the C_{WWW} operator in various scenarios.

	$300\,\text{fb}^{-1}$	$1000\,\text{fb}^{-1}$	$3000\,\text{fb}^{-1}$
$\sqrt{s} = 14$	8 TeV^{-2}	-	2.5 TeV^{-2}
$\sqrt{s} = 33$	-	-	2.0 TeV^{-2}
$\sqrt{s} = 100$	-	1.5 TeV^{-2}	1.0 TeV^{-2}

Table 8: Summary of expected sensitivity to anomalous WWW production at various hadron collider machines, quoted in the terms of approximate 5σ-significance discovery values of C_{WWW}/Λ^2.

References

[1] C. Degrande, N. Greiner, W. Kilian, O. Mattelaer, H. Mebane, et al., *Effective Field Theory: A Modern Approach to Anomalous Couplings (private communication)*, arXiv:1205.4231 [hep-ph].

[2] J. Alwall, M. Herquet, F. Maltoni, O. Mattelaer, and T. Stelzer, *MadGraph 5 : Going Beyond*, JHEP **1106** (2011) 128, arXiv:1106.0522 [hep-ph].

[3] S. Ovyn, X. Rouby, and V. Lemaitre, *DELPHES, a framework for fast simulation of a generic collider experiment*, arXiv:0903.2225 [hep-ph].

[4] A. Avetisyan et al., *Standard Model Background Generation for Snowmass using Madgraph*, arXiv:1307.XXXX [hep-ex].

[5] ATLAS Collaboration, *Measurement of the total ZZ production cross section in proton-proton collisions at $\sqrt{s} = 8$ TeV in 20 fb^{-1} with the ATLAS detector*, Tech. Rep. ATLAS-CONF-2013-020, CERN, Geneva, March, 2013. http://cds.cern.ch/record/1525555.

[6] T. Sjostrand, S. Mrenna, and P. Z. Skands, *PYTHIA 6.4 physics and manual*, JHEP **0605** (2006) 026, arXiv:0603175 [hep-ph].

[7] J. de Favereau, C. Delaere, P. Demin, A. Giammanco, V. Lematre, et al., *DELPHES 3, A modular framework for fast simulation of a generic collider experiment*, arXiv:1307.6346 [hep-ex].

[8] A. Avetisyan et al., *Snowmass Energy Frontier Simulations for Hadron Colliders*, arXiv:1307.XXXX [hep-ex].

[9] J. Anderson et al., *Snowmass Energy Frontier Simulations*, arXiv:1309.1057 [hep-ex].

[10] A. Avetisyan et al., *Methods and Results for Standard Model Event Generation at $\sqrt{s} = 14$ TeV, 33 TeV and 100 TeV Proton Colliders (A Snowmass Whitepaper)*, arXiv:1308.1636 [hep-ex].

[11] A. Avetisyan et al., *Snowmass Energy Frontier Simulations using the Open Science Grid (A Snowmass 2013 whitepaper)*, arXiv:1308.0843 [hep-ex].

[12] O. Schlimpert and B. Feigl, "VBFNLO Utility to Calculate Form Factors." http://www.itp.kit.edu/~vbfnloweb/wiki/doku.php?id=download:formfactor.

[13] ATLAS Collaboration, *A Measurement of WZ production in proton-proton collisions at $\sqrt{s} = 8$ TeV with the ATLAS detector*, Tech. Rep. ATLAS-CONF-2013-021, CERN, Geneva, March, 2013. http://cds.cern.ch/record/1525557.

[14] ATLAS Collaboration, *Studies of Vector Boson Scattering with an Upgraded ATLAS Detector at a High-Luminosity LHC*, Tech. Rep. ATL-PHYS-PUB-2012-005, CERN, Geneva, Nov, 2012. http://cds.cern.ch/record/1496527.

[15] ATLAS Collaboration, *Studies of Vector Boson Scattering And Triboson Production with an Upgraded ATLAS Detector at a High-Luminosity LHC*, Tech. Rep. ATL-PHYS-PUB-2013-006, CERN, Geneva, Jun, 2013. http://cds.cern.ch/record/1558703.

[16] D. Green, *Vector boson fusion and quartic boson couplings*, arXiv:hep-ph/0306160 [hep-ph].

A Comparisons of $W^{\pm}Z/ZZ$ VBS cross sections at ILC and LHC

Dimension-8 operators (TeV^{-4})	14TeV Cross Sections at LHC (pb)	1TeV Cross Sections at ILC (pb)
$f_{T0}/\Lambda^4 = 1$	0.6116	0.01359
$f_{T1}/\Lambda^4 = 1$	0.7437	0.0136
$f_{T2}/\Lambda^4 = 1$	0.5532	0.01357
$f_{M0}/\Lambda^4 = 1$	0.5386	0.01355
$f_{M1}/\Lambda^4 = 1$	0.536	0.01357
$f_{M2}/\Lambda^4 = 1$	0.5365	0.01357
$f_{M3}/\Lambda^4 = 1$	0.5386	0.01355
$f_{S0}/\Lambda^4 = 1$	0.5372	0.01355
$f_{S1}/\Lambda^4 = 1$	0.5342	0.01355
Standard Model	0.5367	0.01356

Table 9: 14 TeV $pp \to WZ + 2j$ (LHC) and 1 TeV $e^+e^- \to WZ + 2j$ (ILC) Vector Boson Scattering process cross section comparisons with dimension-8 operator anomalous coupling coefficients.

Dimension-8 operators (TeV^{-4})	14TeV Cross Sections at LHC (pb)	1TeV Cross Sections at ILC (pb)
$f_{T0}/\Lambda^4 = 1$	0.3266	0.0008081
$f_{T1}/\Lambda^4 = 1$	0.2384	0.0008081
$f_{T2}/\Lambda^4 = 1$	0.1588	0.0007844
$f_{T8}/\Lambda^4 = 1$	0.1935	0.0008983
$f_{T9}/\Lambda^4 = 1$	0.1439	0.0008243
$f_{M0}/\Lambda^4 = 1$	0.138	0.0007597
$f_{M1}/\Lambda^4 = 1$	0.1337	0.0007683
$f_{M2}/\Lambda^4 = 1$	0.136	0.0007346
$f_{M3}/\Lambda^4 = 1$	0.1329	0.0007899
$f_{S0}/\Lambda^4 = 1$	0.1323	0.0007633
$f_{S1}/\Lambda^4 = 1$	0.1328	0.0007628
Standard Model	0.1326	0.0007647

Table 10: 14 TeV $pp \to ZZ + 2j$ (LHC) and 1 TeV $e^+e^- \to ZZ + 2j$ (ILC) Vector Boson Scattering process cross section comparisons with dimension-8 operator anomalous coupling coefficients.